SUPPLEMENTARY MATERIALS

Supplementary Texts:

1. Evaluation of the a posterior NO_X emissions and the bottom-up emission inventory
2. Uncertainty analyses of NO_X emission inversion

Supplementary Figs. S1 to S18

Supplementary Tables S1 to S11

Supplementary Text 1: Evaluation of the a posterior NO_X emissions and the bottom-up emission inventory

With the inversion system combining RETOMI2 constraints and MEIC, the a posterior emissions were estimated to track the short-term variations of NO_X emissions around the events. As shown in Supplementary Table S1, the a posterior emissions of NO_X were 6-29% lower than MEIC, the current best available emission data with the "bottom-up" approach, for the main control periods of all the concern events in YRD. Furthermore, the a posteriori emissions considerably improved the model performance of surface NO_2 and O_3 concentration simulation with WRF-CMAQ (Supplementary Table S2-S3). Specifically, the correlation coefficients (R) between simulation and observation were elevated by about 0.02-0.1 and 0.01-0.41 for NO_2 and O_3, respectively. The normalized mean bias (NMB) and normalized mean error (NME) of NO_2 were reduced from 50% to -4% and from 51% to 23%, respectively, and the analogues numbers were from -22% to 18% and from 33% to 32% for O_3. Note reductions in NO_X emissions during the concern periods always enhanced O_3 concentrations, attributed to a prevailing "VOC-limited" O_3 formation regime in YRD, under which O_3 is more sensitivity to volatile organic compounds (VOC) and can be removed through "titration reaction" with NO[1-3].

Reference:

1. Y. M. Liu, T. Wang, Worsening urban ozone pollution in China from 2013 to 2017-Part 2: The effects of emission changes and implications for multi-pollutant control. Atmos. Chem. Phys. **20**, 6323-6337 (2020).
2. Y. T. Wang, Y. Zhao, Y. M. Liu, Y. Q. Jiang, B. Zheng, J. Xing, Y. Liu, S. Wang, C. P. Nielsen, Sustained emission reductions have restrained the ozone pollution over China. Nat. Geosci. **16**, 967-974 (2023).
3. X. Y. Dong, Y. Gao, J. S. Fu, J. Li, K. Huang, G. S. Zhuang, Y. Zhou, Probe into gaseous pollution and assessment of air quality benefit under sector dependent emission control strategies over megacities in Yangtze River Delta, China. Atmos. Environ. **79**, 841-852 (2013).

Supplementary Text 2: Uncertainty analyses of NO_X emission inversion

The "smearing" effect

For the "top-down" emission inversion, "smearing" effect exists in the mass balance method when correcting the NO_X emissions according to the difference between observed and simulated NO_2 TVCDs in every single grid. It resulted mainly from the insufficient consideration of the regional transport of NO_2 in the NO_X emission inversion, and possibly leads to underestimation in local emissions and overestimation in downwind emissions.

To evaluate the uncertainty from "smearing" effect, we conducted an extra sensitivity test for estimating the a posterior NO_X emissions for the major events, with the same simulation domain as the normal case (Domain 2 in Supplementary Figure S2) but a coarser horizontal resolution of 27×27 km. Supplementary Table S6 shows the comparison of the a posterior NO_X emissions in normal and sensitivity case, indicated by the correlation coefficient (R), NMB and NME between the two estimates. The strong coefficients and small NMEs for all the major events suggest a limited effect of horizontal resolution and thereby "smearing" effect on emission inversion.

The sensitivity test of sector-level emission decomposition

The uncertainty of sector-level emission estimation was tested by changing the criterion of defining the main emission sectors of the grid cells. In the normal case, we defined a sector as the main sector for individual simulation grid cell if it accounted for more than 50% of total emissions (Methods). Here we changed the criterion to 40% and 60%, and repeated the decomposition of sector-level emissions respectively.

Supplementary Table S7 shows the comparison of the inversed sector-level emissions with different criteria, indicated by R, NMB and NME between different estimates. The large R (>0.8 for most cases) and small NMEs (<20%) suggest the uncertainty from changing criterion of defining main emission sectors was moderate.

The sensitivity test of β (response of NO_2 TVCDs to changing NO_X emissions)

When estimating the response of NO_2 TVCDs to changing NO_X emissions, we applied a 10% perturbation in NO_X emissions (Methods and Eq. 6). To test this uncertainty, we changed the NO_X emission perturbation from 20% to 60%, and repeated the NO_X emission inversion for 2014 NMD as an example. As shown in Supplementary Table S11, the variability of β with emission perturbation ranging 20%-60% was within 10%, compared to that with emission perturbation of 10%. Therefore, the value of β was not sensitive to varying emission perturbation.

Supplementary Figures

Fig. S1. Host and neighboring cities of the major events in the YRD region. We defined neighboring cities as one that borders the host city. The darker colors (green, blue, orange) represent host cities (Nanjing, Shanghai, and Hangzhou), and the lighter colors represent neighboring cities.

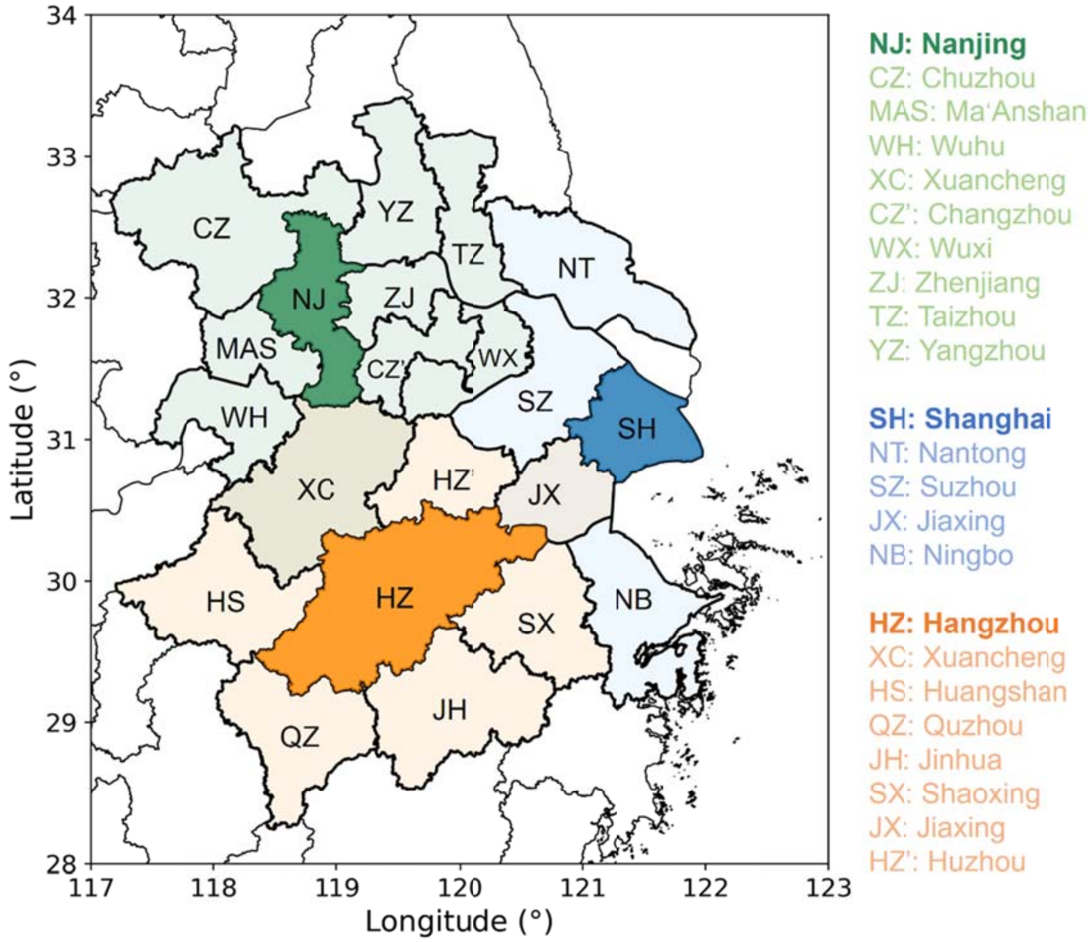

Fig. S2. Modeling domain of WRF-CMAQ and the locations of meteorological, air quality, and MAX-DOAS measurement stations in YRD. A nested WRF-CMAQ model is applied at the horizontal resolution of 27 × 27 km (Domain 1) and 9 × 9 km (Domain 2). Domain 1 provided initial and boundary fields for Domain 2, where the NO_X emissions were inversed. The MAX-DOAS measurements were available at monthly level in Hefei (117.16ºE, 31.91ºN), Nanjing (118.95ºE, 32.118ºN) and Shanghai (120.98 ºE, 31.09ºN), and at daily level in Xuzhou (117.14º E, 34.22º N).

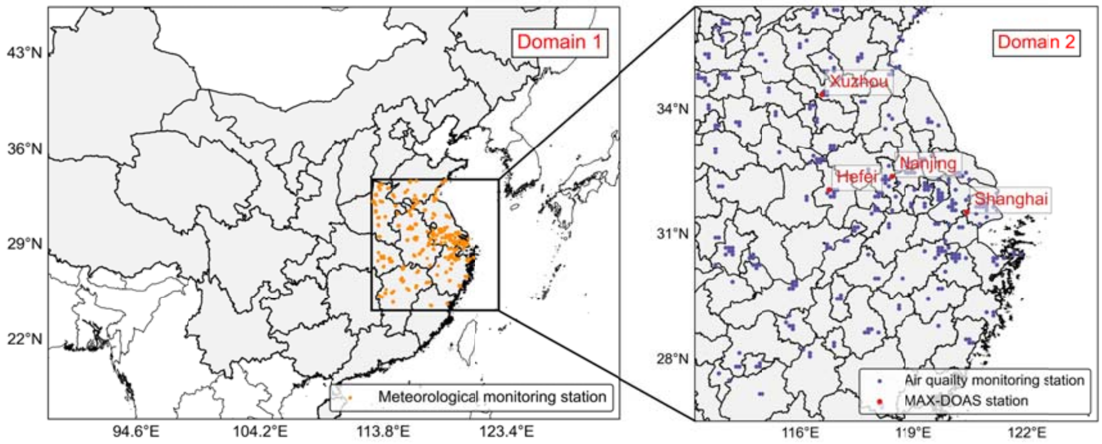

Fig. S3. The spatial distribution of standard deviations of NO_2 TVCDs in POMINO and RETOMI2, and the difference between them during the main control periods of major events. The horizontal resolution is 0.05°×0.05° (Original POMINO data were downscaled by bilinear interpolation).

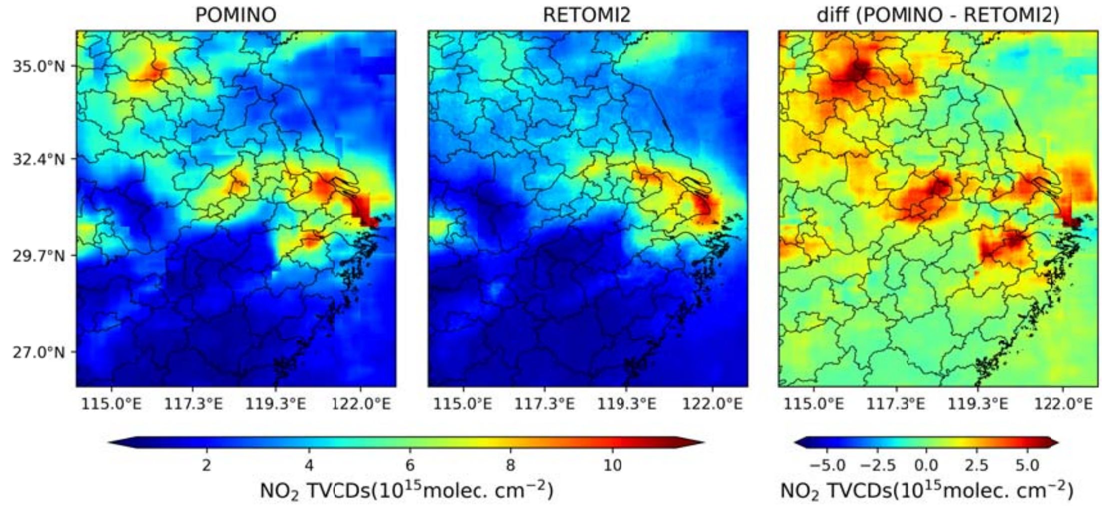

Fig. S4. Monthly temporal variation of NO_2 TVCDs from satellite data (RETOMI2 and POMINO) and ground-based observations from MAX-DOAS at Hefei (117.16°E, 31.91°N; from January 2014 to December 2016, red curves with dots), Nanjing (118.95°E, 32.118°N; from October 2015 to December 2016, blue curves with dots) and Shanghai (120.98 °E, 31.09°N; from April to December 2016, green curves with dots).

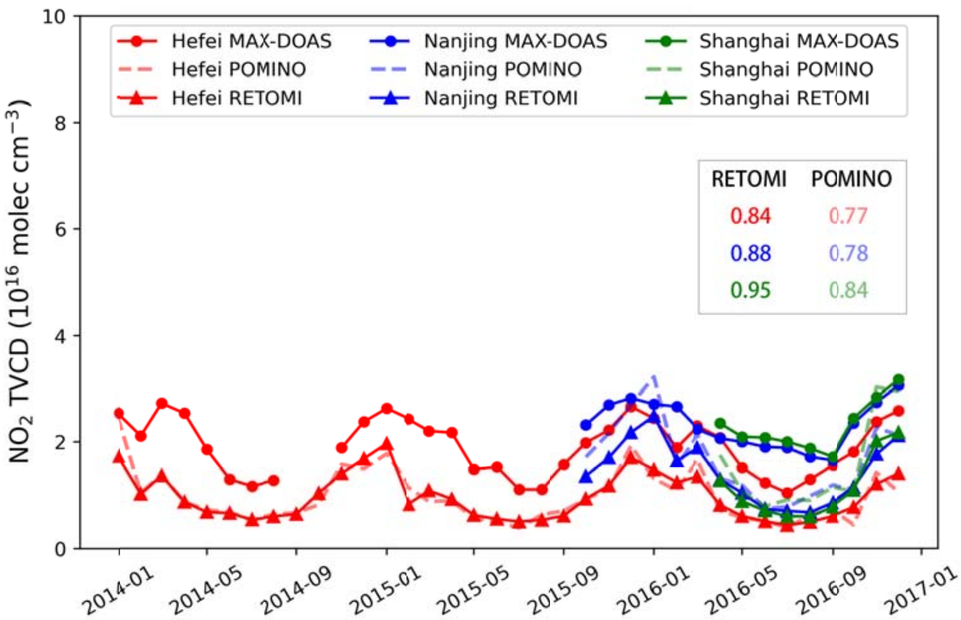

Fig. S5. Interannual trends of NO_X emissions from MEIC during 2008-2020 for YRD (A, E), Shanghai (B, F), Nanjing (C, G) and Hangzhou (D, H). The black dotted lines represent annual total NO_X emissions. The red, green and light blue bars represent the emissions from industrial, power and transportation sectors, respectively. The red, green and light blue dotted lines indicate the relative change in emissions from 2008 for the industry, electricity and transportation sectors, respectively.

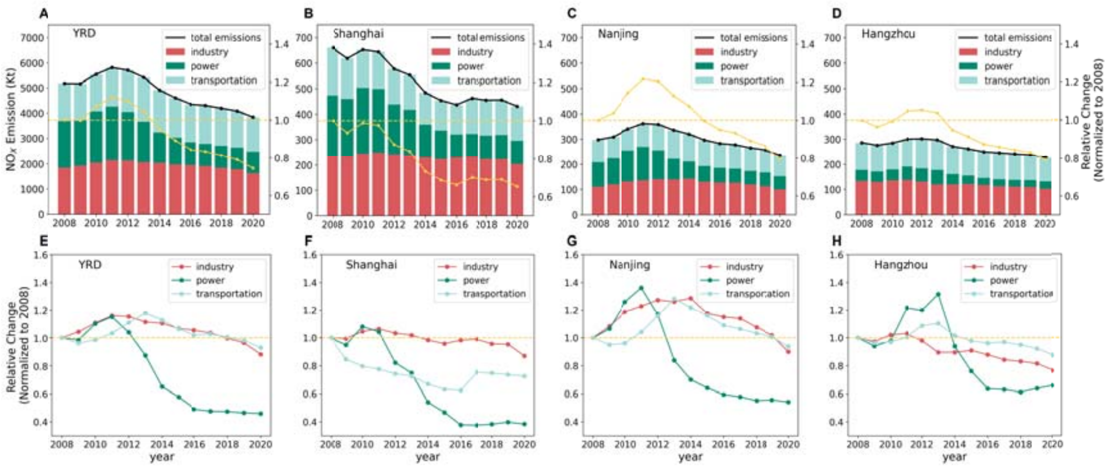

Fig. S6. Daily variation of observed surface NO_2 concentration in Nanjing in August 2013 and August 2014. The data for August 2013 and August 2014 are indicated in blue and orange respectively. Observations during the event are indicated with red dots.

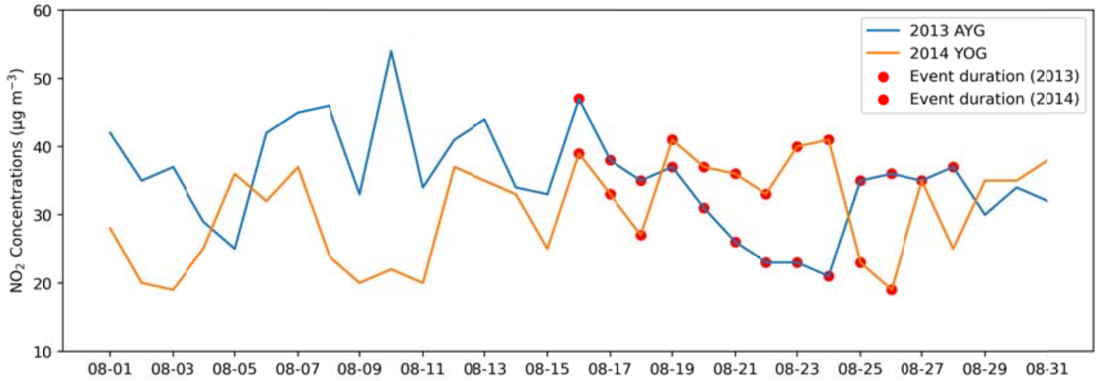

Fig. S7. Difference of simulated hourly mean meteorological conditions during the 2013 AYG and 2014 YOG. Difference is indicated as meteorological factors on 16-28 August 2013 minus meteorological factors on 16-28 August 2014. (A) Temperature at 2m (T2), (B) Relative humidity (RH) at 2m, (C) Planetary boundary layer height (PBLH), (D) Surface pressure (SP), (E) Wind speed and direction at 10-meter in 2013 AYG, (F) Wind speed and direction at 10-meter in 2014 YOG. The boxes in the upper right corner show the bias of mean value (A-D) or the mean value of wind speed (E, F). The black box in each plot shows the location of Nanjing.

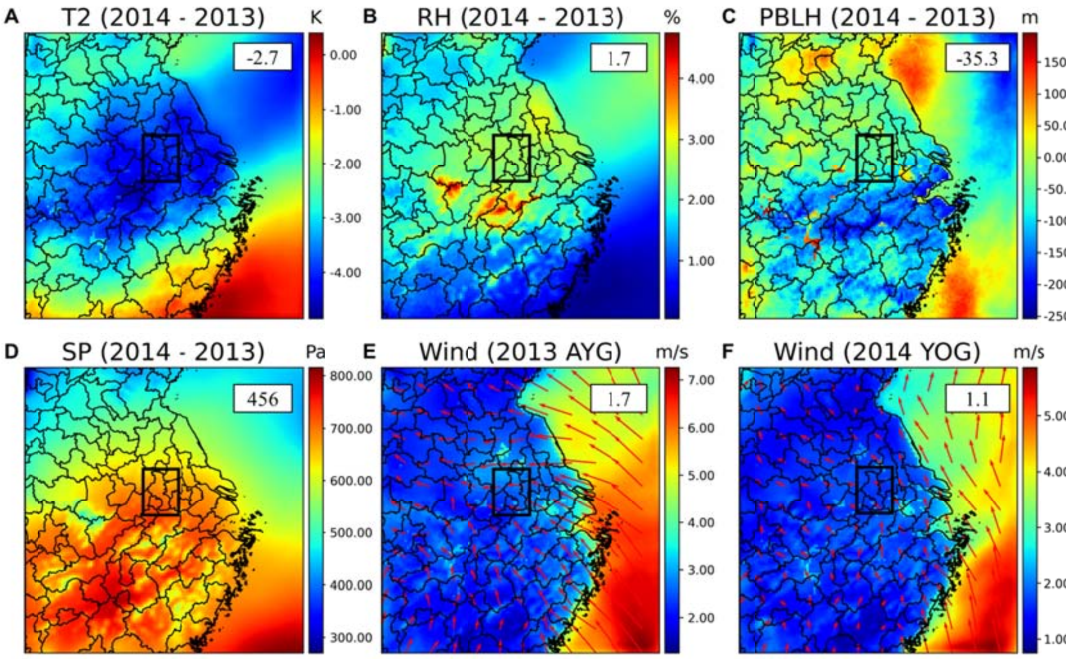

Fig. S8. Time series of daily observed concentrations of air pollutants (SO_2, NO_2, CO, O_3, $PM_{2.5}$ and PM_{10}), meteorological parameters (temperature, rainfall, wind speed at 10-meter, relative humidity, sunshine duration and PBLH) and the a NO_X posterior emissions in Hangzhou from August to September 2016. The red shade indicates the G20 summit period (Sep. 4 - Sep. 5, 2016). The grey shade indicates Phase II (Aug. 28 - Sep. 6, 2016) in main control period of 2016 G20.

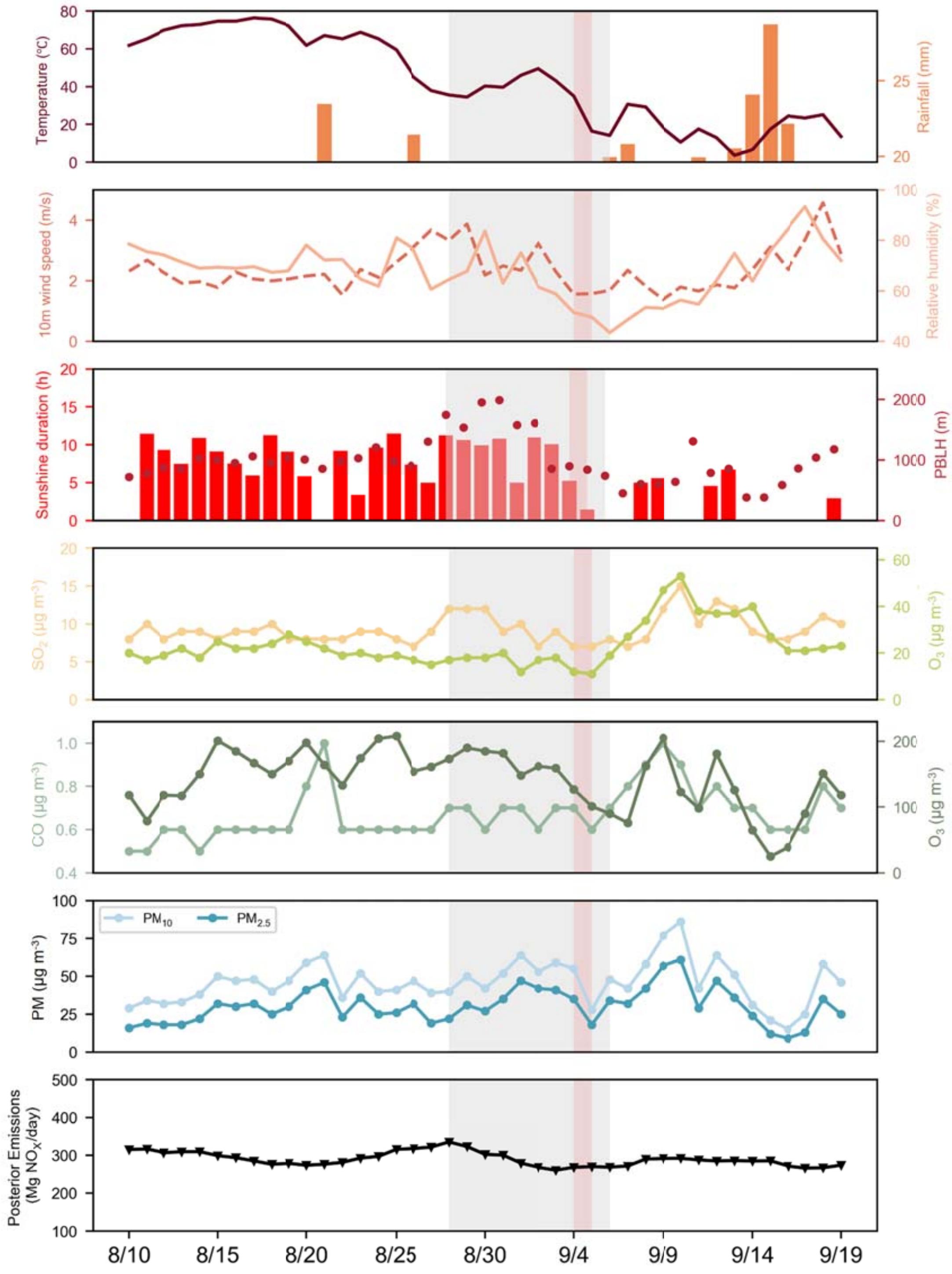

Fig. S9. The timeline of major events and long-term air pollution prevention actions and mechanisms.

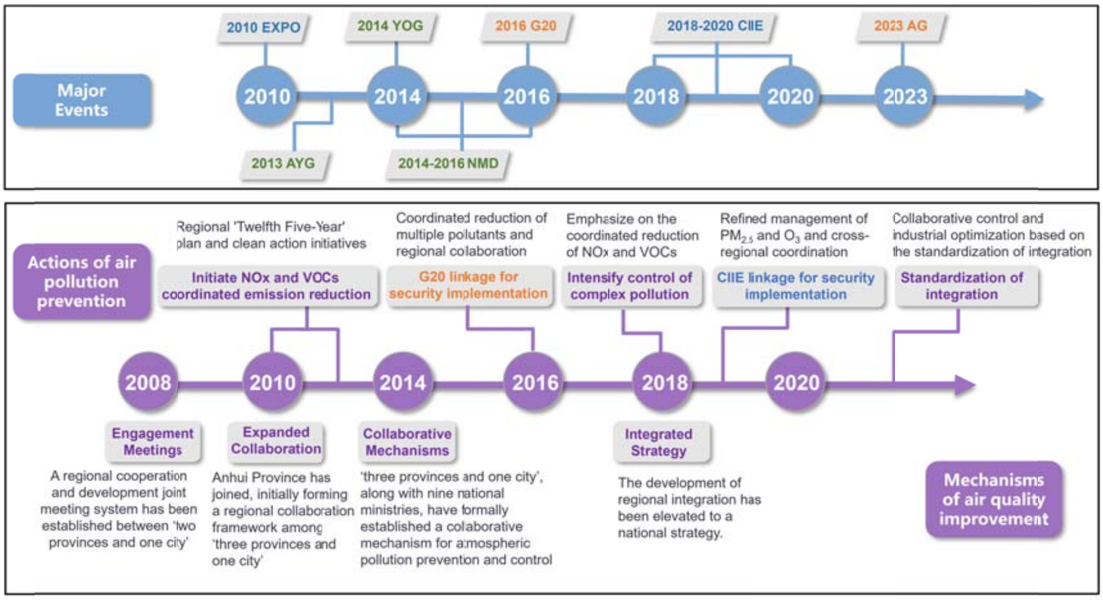

Fig. S10. The methodological flowchart of the study.

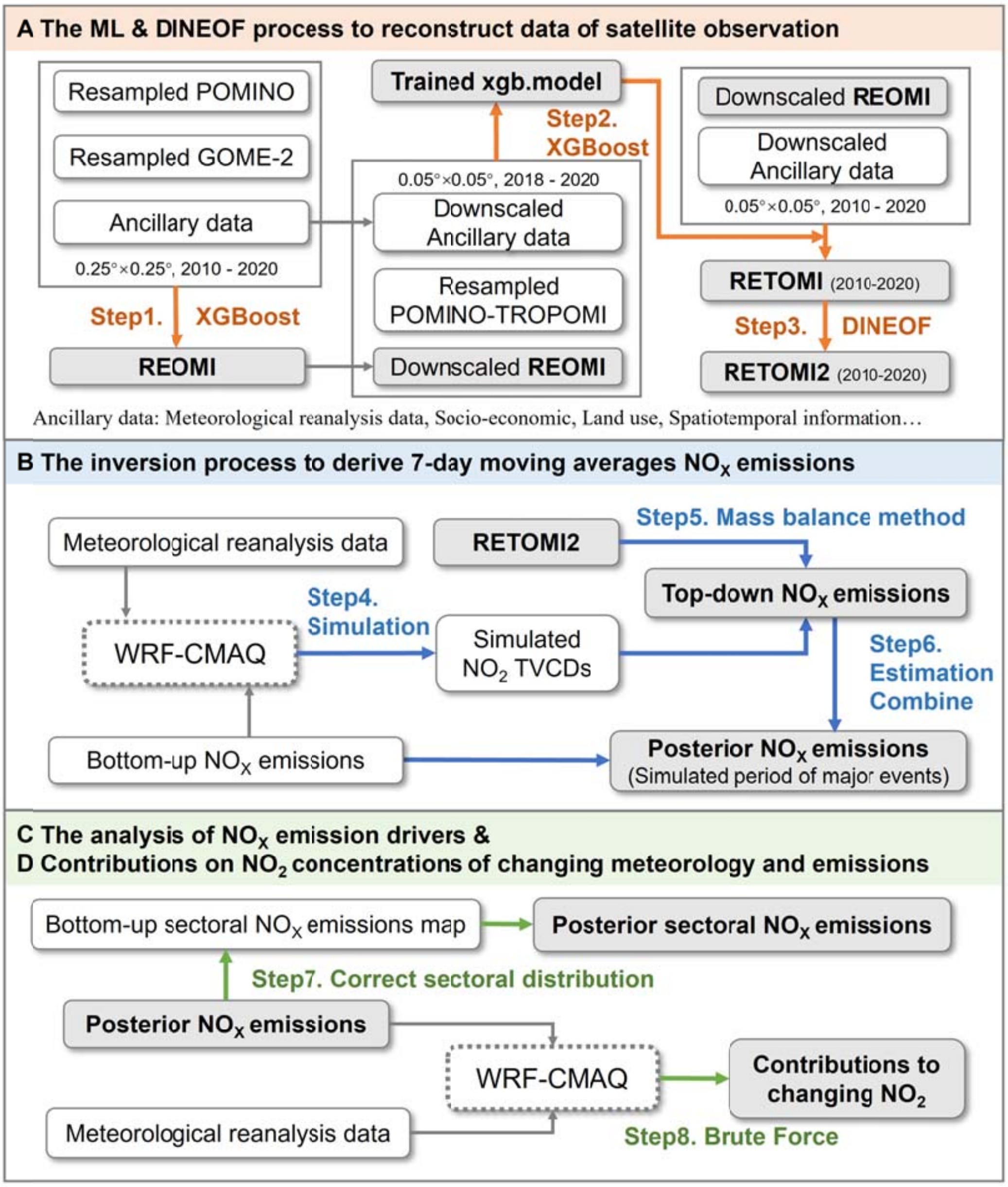

Fig. S11. Scatterplot of historical NO_2 TVCDs from POMINO-TROPOMI and RETOMI (Jul.1, 2018 to Dec. 31, 2020). The slope and intercept were applied to adjust POMINO-TROPOMI data during the simulation period of 2023 AG.

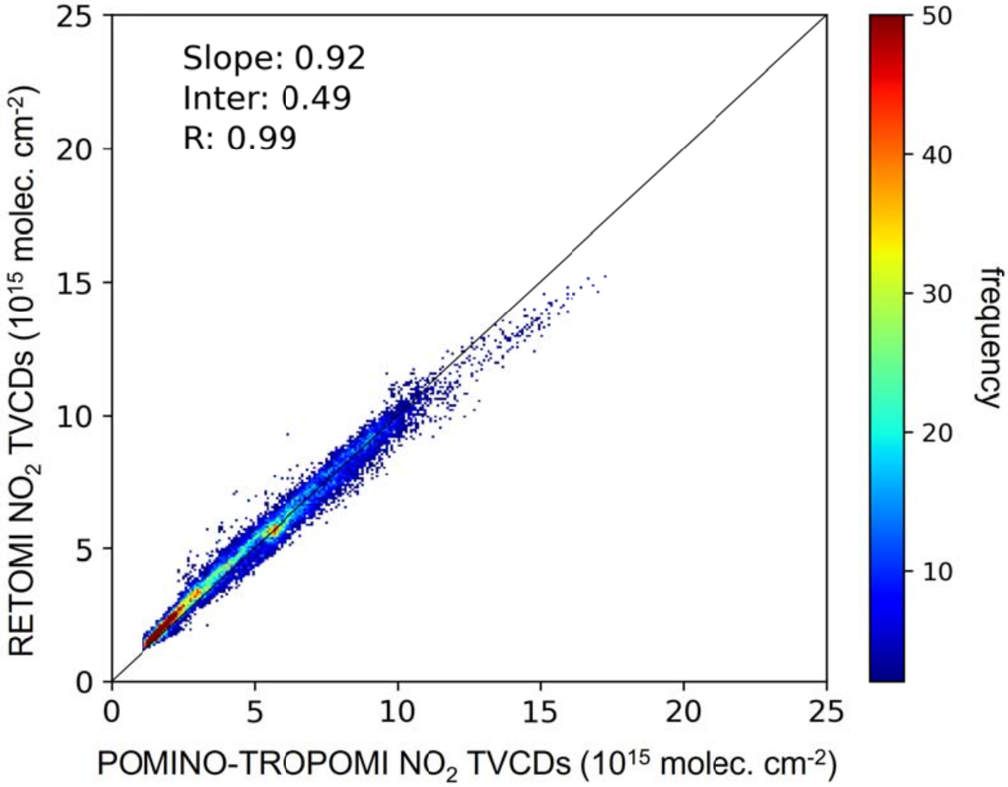

Fig. S12. Scatterplot of historical averaging kernels of RETOMI (REAK) and POMINO-TROPOMI (Jul.1, 2018 - Dec. 31, 2020). The slope and intercept were applied to adjust the AKs of POMINO-TROPOMI during the simulation period of 2023 AG.

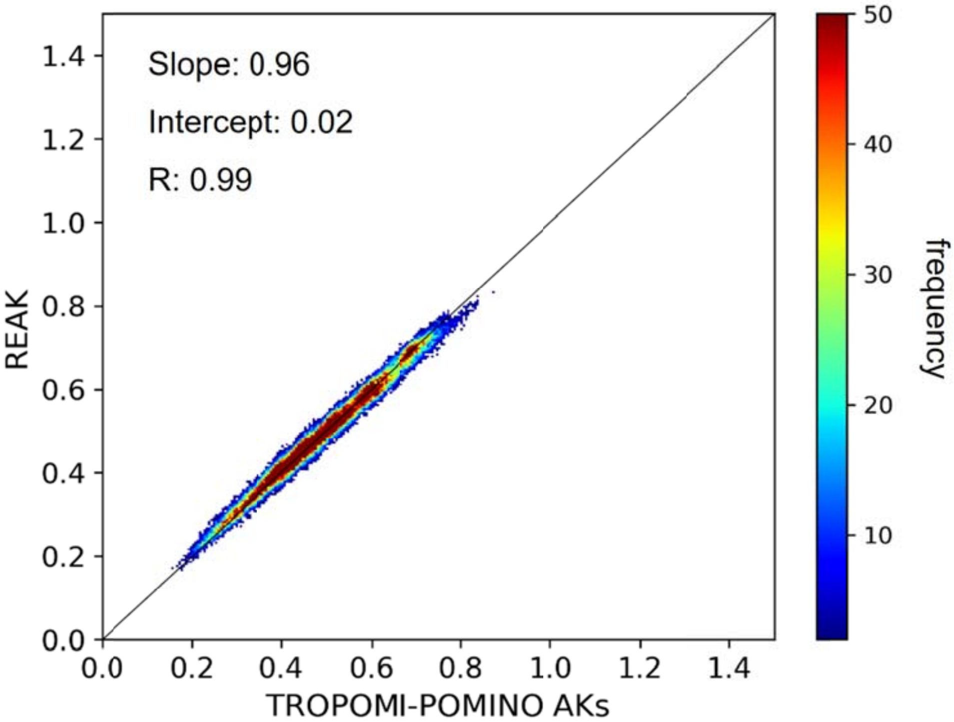

Fig. S13. Scatterplot of NO_2 TVCDs from REOMI and POMINO (left and right panels for each year indicate the training and validation dataset, respectively).

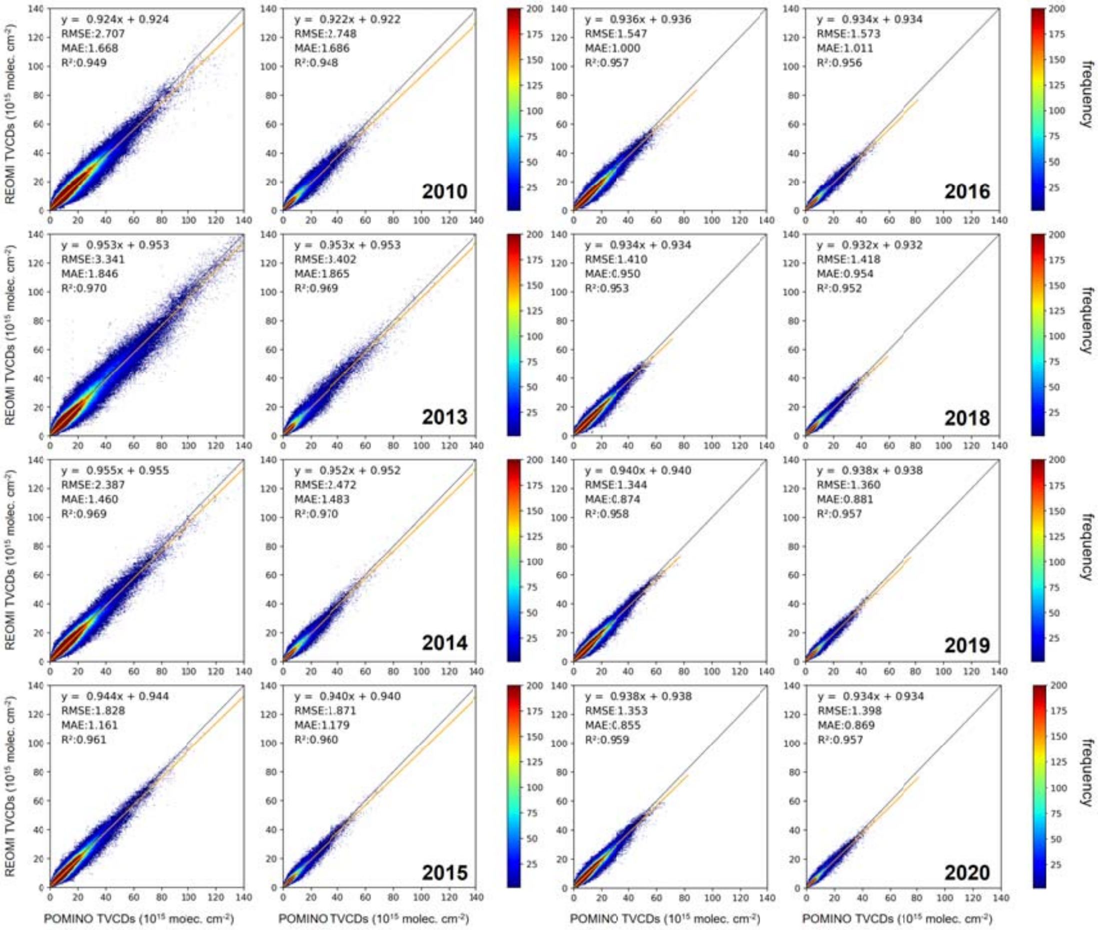

Fig. S14. Scatterplot of NO_2 TVCDs from RETOMI and POMINO-TROPOMI (left and right panel indicate the training and validation dataset, respectively).

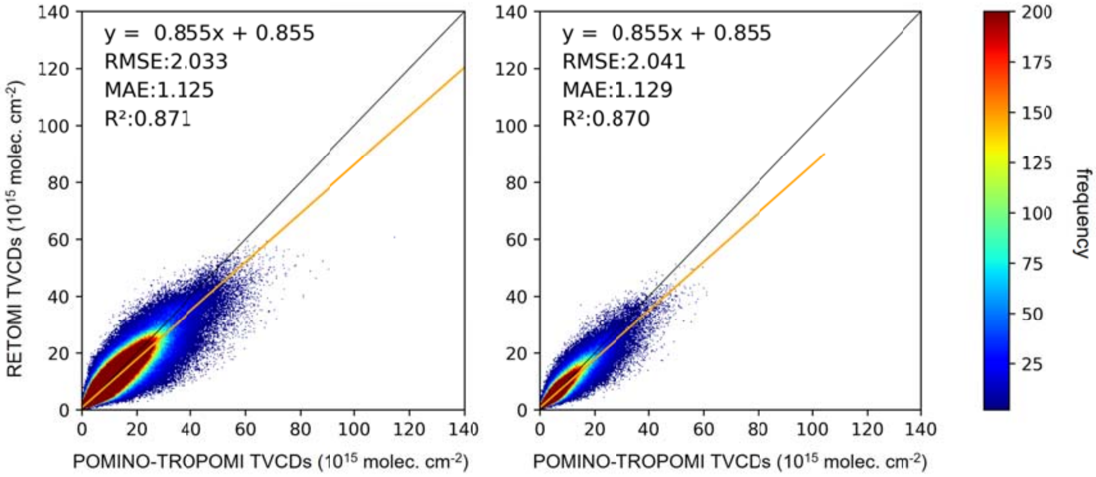

Fig. S15. Scatterplot of REAK and POMINO-TROPOMI AKs (left and right panels indicate train and test dataset, respectively).

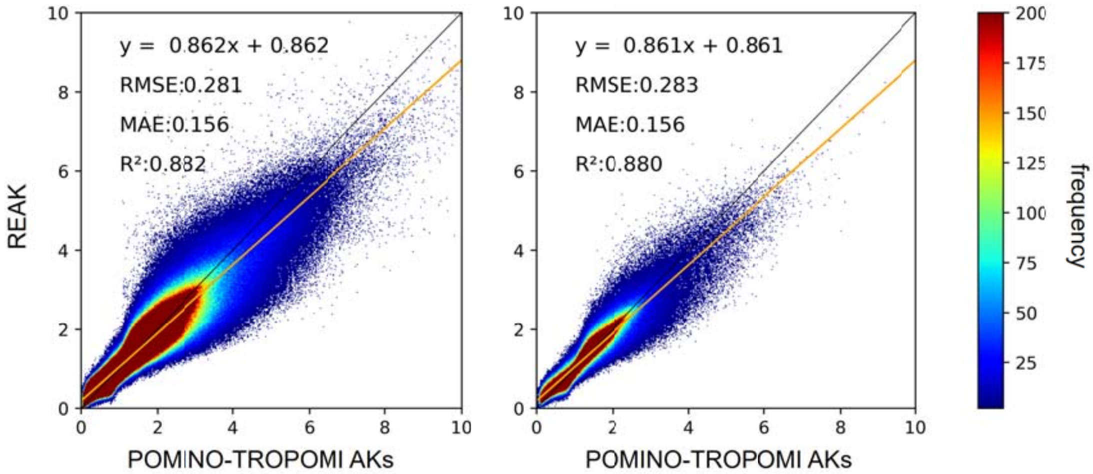

Fig. S16. The influence of Expected Error (*RMSE*) by number of EOFs modes (*P*) in DINEOF. Take a specific event (2014 NMD) as an example. P_b is the specific number of EOFs modes set to meet a condition where the *RMSE* change is less than 1%. In this case, P_b was set as 56 (*RMSE*=0.923), the change in *RMSE* between *P*=56 and *P*=55 is less than 1%.

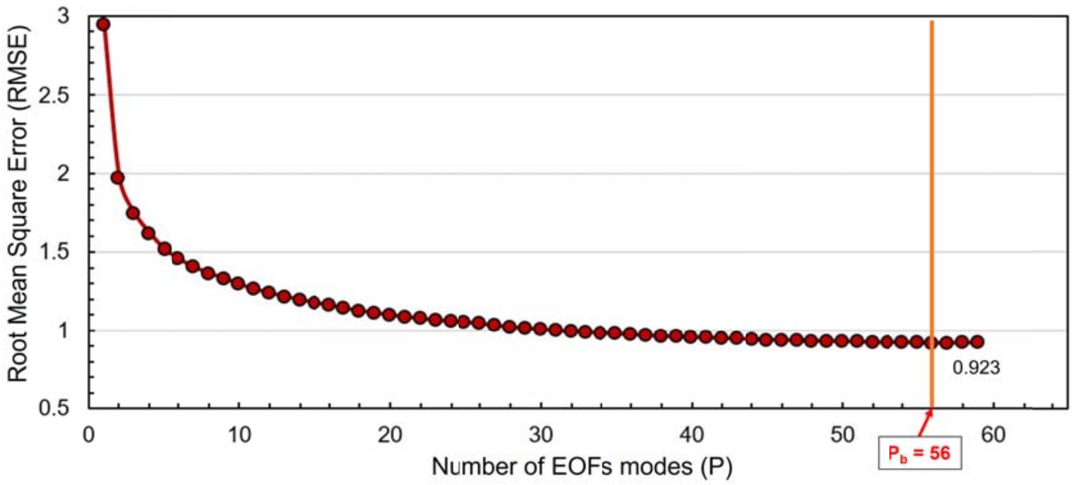

Fig. S17. The spatial distribution of β (the sensitivity of NO_2 TVCDs to changing NO_X emissions) at YRD region during main control period of major events.

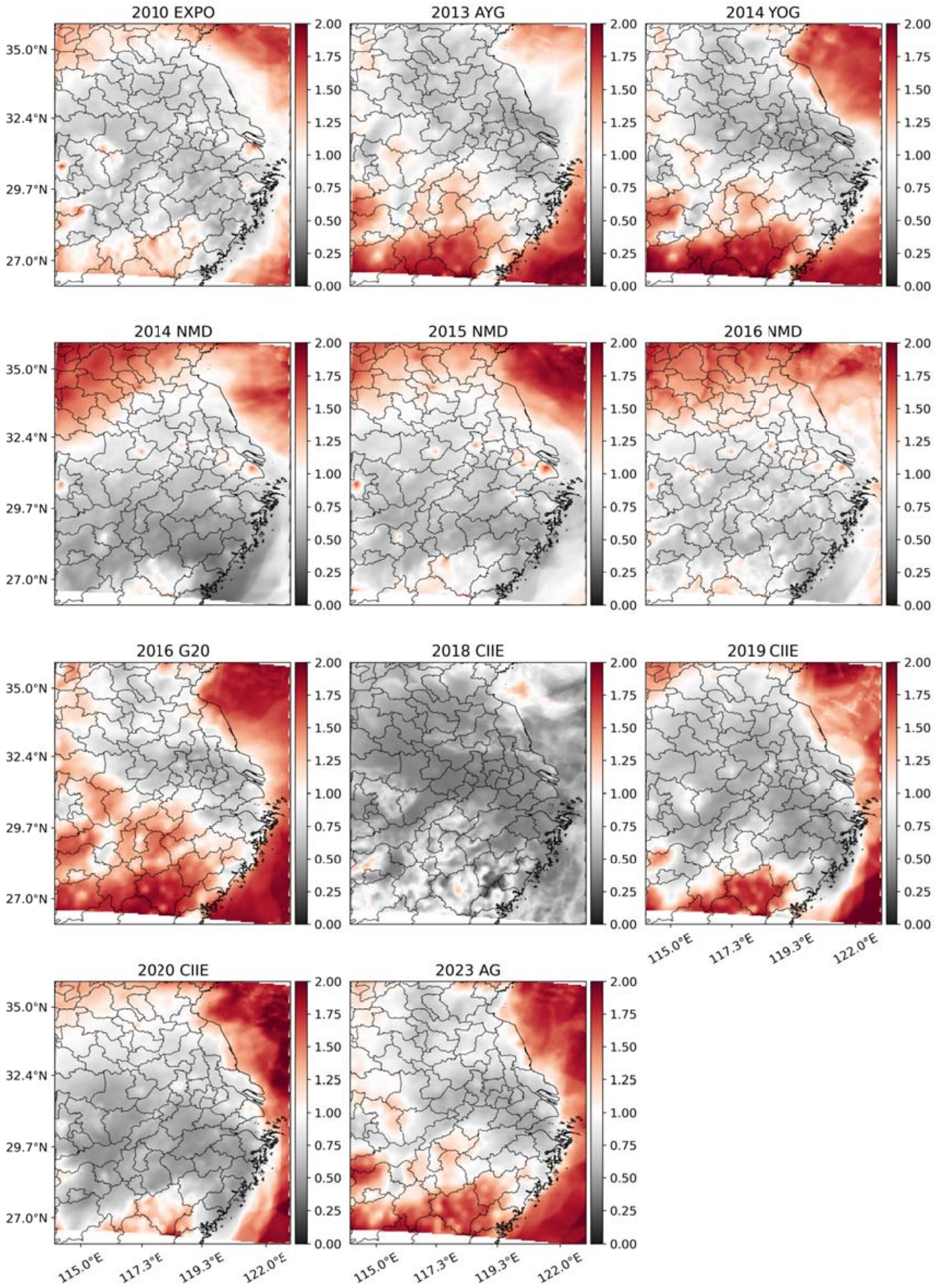

Fig. S18. Scatterplot of NO_2 TVCDs from RETOMI2 and WRF-CMAQ simulation by month.

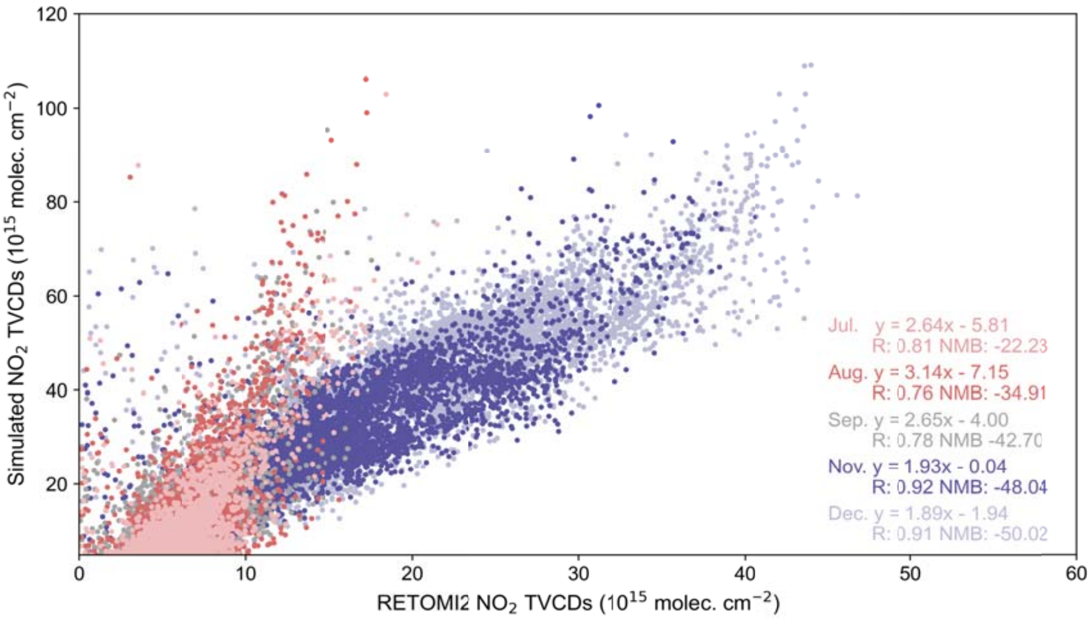

Supplementary Tables

Table S1. The bottom-up (MEIC) and the a posterior NO_X emissions (units: Gg NO_X) and the relative difference (Diff) between them in YRD during the simulation period of the 11 major events.

Event	YRD (Gg NO_X)			Host city (Gg NO_X)			
	MEIC	The a posterior	Diff	City	MEIC	The a posterior	Diff
2010 EXPO	5651	4714	-17%	Shanghai	351	250	-41%
2013 AYG	1798	1608	-11%	Nanjing	48	38	-24%
2014 YOG	1628	1467	-10%	Nanjing	46	34	-33%
2014 NMD	1078	764	-29%	Nanjing	30	20	-47%
2015 NMD	1022	777	-24%	Nanjing	28	18	-53%
2016 G20	980	773	-21%	Hangzhou	27	20	-33%
2016 NMD	1432	1321	-8%	Nanjing	40	34	-17%
2018 CIIE	844	792	-6%	Shanghai	46	40	-15%
2019 CIIE	838	746	-11%	Shanghai	49	34	-46%
2020 CIIE	848	748	-12%	Shanghai	50	35	-44%
2023 AG	1361	1162	-15%	Hangzhou	42	35	-21%

Table S2. The model performance of surface NO_2 concentration with the a posterior emissions and the bottom-up estimates (MEIC). Numbers in red indicate that the simulation of the a posteriori emission performed better than MEIC. The evaluation period was the main control period of major events.

Event	Emission data	Observation mean (YRD)	Simulation Mean (YRD)	R	NMB	NME
2014 YOG	MEIC	29.21	51.16	0.75	76.50	76.73
	Posterior		37.11	0.75	1.05	27.35
2014 NMD	MEIC	48.02	63.81	0.75	32.89	34.11
	Posterior		37.97	0.81	-20.93	23.26
2015 NMD	MEIC	43.13	61.40	0.69	43.86	43.94
	Posterior		38.53	0.67	-10.67	22.28
2016 G20	MEIC	22.62	39.98	0.68	75.98	77.25
	Posterior		24.01	0.70	6.14	34.85
2016 NMD	MEIC	47.08	59.14	0.68	25.62	29.22
	Posterior		38.05	0.62	-19.18	26.43
2018 CIIE	MEIC	37.32	54.54	0.69	46.14	46.89
	Posterior		32.40	0.78	-13.17	19.99
2019 CIIE	MEIC	36.42	52.24	0.80	43.46	44.56
	Posterior		37.74	0.84	3.62	21.04
2020 CIIE	MEIC	34.67	49.86	0.73	43.78	45.21
	Posterior		37.19	0.82	7.24	20.47
2023 AG	MEIC	27.29	43.28	0.84	58.58	59.75
	Posterior		30.20	0.86	10.66	12.42

Table S3. The same as Table S2 but for O_3 simulation.

Event	Emission data	Observation mean (YRD)	Simulation mean (YRD)	R	NMB	NME
2014 YOG	MEIC	65.75	56.09	0.87	-14.68	23.15
	Posterior		72.56	0.88	9.68	22.12
2014 NMD	MEIC	70.85	60.15	0.85	-15.11	23.14
	Posterior		70.75	0.85	-0.14	22.36
2015 NMD	MEIC	47.13	22.22	-0.44	-52.84	62.56
	Posterior		47.41	0.85	55.81	56.54
2016 G20	MEIC	30.47	19.20	0.72	-37.00	40.11
	Posterior		44.98	0.74	48.09	52.98
2016 NMD	MEIC	35.85	24.51	0.71	-31.62	38.10
	Posterior		45.84	0.77	27.87	36.77
2018 CIIE	MEIC	44.85	36.54	0.77	-18.53	32.42
	Posterior		44.37	0.72	-1.08	32.81
2019 CIIE	MEIC	46.07	43.99	0.86	-4.53	25.06
	Posterior		54.41	0.88	18.09	27.06
2020 CIIE	MEIC	45.07	33.99	0.84	-24.57	31.94
	Posterior		49.08	0.87	8.90	23.62
2023 AG	MEIC	69.01	68.40	0.84	-0.87	23.13
	Posterior		69.08	0.85	0.10	22.16

Table S4. The short-term emission control measures for the major events.

Event	Main control period	Specific measures
2010 EXPO	Apr. 1 - Oct. 1, 2010	**Point sources:** All coal-fired boilers, power plants and key industrial factories within a 300-kilometer radius of the Expo site were under priority control. Clean power generation took priority during high pollution period. **Area sources:** Waste straw burning and construction dust emissions were strictly controlled. **Mobile sources:** High-emission vehicles were eliminated or restricted from entering the Expo venue. Zero-emission public transportation systems and tightened vehicle emission standards were implemented.
2013 AYG	Aug. 1 - Aug. 30, 2013	**Point sources:** Nearly 60 heavy industrial factories were shut down. Power generation was reduced. The use of coal-fired boilers was prohibited. **Area sources:** The work at all construction sites was stopped. The control of restaurant fume emissions was strengthened. Road cleaning was strengthened. **Mobile sources:** High-emission vehicles were banned from the city.
2014 YOG	Phase I: Sep. 15 - Sep. 31, 2014	**Point sources:** All coal-fired factories were shut down. **Area sources:** The work on one-third of construction sites was stopped. **Mobile sources:** The parking fees in downtown increased sevenfold.
	Phase II: Aug. 1 - Aug. 30, 2014	**Point sources:** Twenty percent of manufacturing was reduced for heavy industrial factories. **Area sources:** The work at all construction sites was stopped (Aug.16-31). Openair barbecue was stopped **Mobile sources:** High-emission vehicles were banned from entering the city. In total 900 electric buses and 500 taxis were put into operation.
2014 NMD	Nov. 17 - Dec. 17, 2014	**Point sources:** The removal efficiencies of air pollutant control facilities were elevated, including gas desulphurization, selective catalytic reduction, and dust collectors. A number of heavy industrial factories were shut down. **Area sources:** The work at all construction sites was stopped. Road cleaning was strengthened. **Mobile sources:** All yellow-labeled and high-emission vehicles were banned from entering the city. Thirty percent of government vehicle use was stopped.

Table S4. (Continued Table)

Event	Main control period	Specific measures
2015 NMD	Dec. 7 - Dec. 15, 2015	**Point sources:** The removal efficiencies of air pollutant control facilities were elevated. Thirty-one heavy industrial factories were shut down. Key factories reduced manufacturing by 30%. **Area sources:** The work at all construction sites was stopped. Road cleaning was strengthened. **Mobile sources:** Heavy-duty trucks were prohibited from entering the city. **Emergency Control Measures:** Special control measures were implemented during the pollution period. Restrictions on manufacturing were elevated for industries. Further measures were taken to control emissions from vehicles, ships, and dust pollution (Dec. 11 - Dec. 13, 2015).
2016 G20	Phase I: Aug. 1 - Aug. 27, 2016	**Point sources:** Heavy industrial factories were shut down or required to reduce production. **Area sources:** The work at all construction sites was stopped (Aug. 25 - Sep. 6).
	Phase II: Aug. 28 - Sep. 6, 2016	**Point sources:** Same as Phase I. **Mobile sources:** Vehicles from outside Hangzhou were banned from entering the city. Odd-even traffic rule was implemented (Aug. 28 - Sep. 3).
2016 NMD	Dec. 9 - Dec. 13	The same as 2015 NMD.
2018 CIIE 2019 CIIE 2020 CIIE	Oct. 27 - Nov. 10 Oct. 27 - Nov. 10 Nov. 1 - Nov. 10	**Point sources:** The upgrade of coal-fired boilers and production restrictions for key enterprises were strengthened. **Area sources:** Waste straw burning and construction dust emissions were strictly controlled. Road cleaning was strengthened. **Mobile sources:** The number of on-road vehicles was restricted. Pollution prevention and control of high-emission vehicles and non-road machinery was strengthened.
2023 AG	Sep. 10 – Oct. 8	**Point sources:** The removal efficiencies of air pollutant control facilities were elevated. **Area sources:** Road cleaning was strengthened. **Mobile sources:** The number of on-road vehicles was restricted. Pollution prevention and control of high-emission vehicles and non-road machinery was strengthened. **Emergency Control Measures:** Platform was established to detect and track the hotspot of pollution.

Table S5. The simulation periods used to distinguish between meteorological and emission contributions (P1 and P2). P2 included the full period of main control for each event, with an exception of 2010 EXPO, for which April 2010 was selected as P2 to save computational cost. P1 was the period before P2 with the same duration as P2.

Event	P1	P2
2010 EXPO	Mar. 2 - Mar. 31, 2010	Apr. 1 - Apr. 30, 2010
2013 AYG	Jul. 2 - Jul. 31, 2013	Aug. 1 - Aug. 30, 2013
2014 YOG	May. 28 - Jul. 14, 2014	Jul. 15 - Aug. 31, 2014
2014 NMD	Oct. 17 - Nov. 16, 2014	Nov. 17 - Dec. 17, 2014
2015 NMD	Nov. 28 - Dec. 6, 2015	Dec. 7 - Dec. 15, 2015
2016 G20	Jun. 25 - Jul. 31, 2016	Aug. 1 - Sep. 6, 2016
2016 NMD	Dec. 4 - Dec. 8, 2016	Dec. 9 - Dec. 13, 2016
2018 CIIE	Oct. 12 - Oct. 26, 2018	Oct. 27 - Nov. 10, 2018
2019 CIIE	Oct. 12 - Oct. 26, 2019	Oct. 27 - Nov. 10, 2019
2020 CIIE	Oct. 22 - Oct. 31, 2020	Nov. 1 - Nov. 10, 2020
2023 AG	Aug. 12 - Sep. 9, 2023	Sep. 10 - Oct. 8, 2023

Table S6 Comparison of the a posteriori emissions inversed at two horizontal resolutions (27×27 km and 9×9 km) during the main control periods of the 11 major events.

Event	R	NMB (%)	NME (%)
2010 EXPO	0.86	1.21	4.04
2013 AYG	0.95	-0.20	1.39
2014 YOG	0.91	0.89	2.88
2014 NMD	0.89	-0.07	2.28
2015 NMD	0.87	0.64	4.57
2016 G20	0.91	0.50	3.15
2016 NMD	0.93	0.78	2.93
2018 CIIE	0.98	0.49	2.24
2019 CIIE	0.85	0.99	3.07
2020 CIIE	0.91	-0.28	1.85
2023 AG	0.96	1.36	4.26

Table S7. Variability in the a posterior NO_X emissions at the sector level with different criteria to identify the main emissions sector for individual grid cells. Comparisons were conducted between the estimates with a criterion of 40% and 50%, and between the estimates with a criterion of 60% and 50% (see explanation of the criterion in Supplementary Texts).

Event	Sector	40% versus 50%			60% versus 50%		
		R	NMB (%)	NME (%)	R	NMB (%)	NME (%)
2010 EXPO	Industry	0.91	-3.61	8.64	0.96	-8.25	8.93
	Power	0.95	3.38	9.18	0.96	15.69	15.81
	Transportation	0.98	0.97	3.19	0.97	-8.00	8.95
2013 AYG	Industry	0.93	-1.38	2.57	0.89	0.12	2.56
	Power	1.00	0.08	0.51	0.99	0.25	1.32
	Transportation	0.98	0.64	1.12	0.98	-0.14	1.05
2014 YOG	Industry	0.98	0.43	1.20	0.95	3.69	3.94
	Power	1.00	-0.21	0.45	1.00	0.38	1.16
	Transportation	1.00	-0.21	0.61	0.98	-2.32	2.46
2014 NMD	Industry	0.99	-0.21	2.63	0.98	-3.71	4.72
	Power	1.00	0.13	0.85	0.99	-3.64	3.70
	Transportation	1.00	0.04	1.48	0.99	3.31	3.81
2015 NMD	Industry	0.99	0.87	2.58	0.97	-1.03	5.87
	Power	0.99	1.27	2.24	0.98	-6.35	6.54
	Transportation	1.00	-0.59	1.32	0.99	2.63	4.31
2016 NMD	Industry	0.99	0.04	3.89	0.99	-5.39	6.28
	Power	1.00	-0.76	2.11	1.00	-2.71	3.12
	Transportation	1.00	0.10	2.02	1.00	3.73	3.87
2016 G20	Industry	0.96	0.71	1.53	0.43	17.50	17.50
	Power	0.99	0.48	0.85	0.94	-11.61	11.61
	Transportation	1.00	-1.08	1.46	0.92	-19.10	19.10
2018 CIIE	Industry	0.96	4.25	4.25	0.92	0.12	2.07
	Power	0.99	-3.60	3.60	0.98	0.02	1.42
	Transportation	0.91	-2.77	2.86	0.97	-0.16	1.31
2019 CIIE	Industry	0.90	7.61	8.84	0.92	5.69	7.83
	Power	0.86	-12.04	14.67	0.95	-3.36	4.75
	Transportation	0.92	0.07	6.17	0.97	-3.44	4.67
2020 CIIE	Industry	0.82	14.01	14.52	0.85	1.39	8.40
	Power	0.93	-15.64	15.64	0.92	-0.55	4.00
	Transportation	0.85	-2.35	8.91	0.98	-0.68	3.55
2023 AG	Industry	1.00	1.43	1.48	0.94	4.12	4.39
	Power	1.00	-0.24	0.68	0.96	-1.69	2.76
	Transportation	1.00	-1.33	1.33	0.97	-3.23	3.48

Table S8. Summary of data used in REOMI development (Step 1). POMINO and GOME-2 data were resampled to 0.25° ×0.25° through Level-2 products. Other ancillary data in this table were downscaled to the same horizontal resolution of 0.25° ×0.25° by bilinear interpolation. POMINO was the target variable of the model (green shade).

Data type	Variable	Abbreviation	Unit	Period
POMINO	NO_2 TVCDs	pomino	molec. cm^{-2}	2010, 2013-2016, 2018-2020
GOME-2a	NO_2 TVCDs	gome	molec. cm^{-2}	2010
GOME-2b	NO_2 TVCDs	gome	molec. cm^{-2}	2013-2016, 2018-2020
Meteorology	2m temperature	t2m	K	2010, 2013-2016, 2018-2020
	Boundary layer height	blh	m	
	100-meter eastward wind	u100	m s^{-1}	
	100-meter northward wind	v100	m s^{-1}	
	10-meter eastward wind	u10	m s^{-1}	
	10-meter northward wind	v10	m s^{-1}	
	Surface pressure	sp	hPa	
	Total column ozone concentration	tco3	du	
	2-meter dew point temperature	d2m	K	
	Total Trop. column water	tcw	g cm^{-2}	
	Total column water vapor	tcwv	g cm^{-2}	
Socio-economic	Gridded population	pop	people/grid	
Land use	Proportion of crop	cropland	%	
	Proportion of impervious surface	impervious surface	%	
	Proportion of water	water	%	
	Proportion of forest	forest	%	
Spatiotemporal information	Longitude	lon	°	
	Latitude	lat	°	
	Day of year	doy	-	
	Day of week	dow	-	

Table S9. Summary of data used in RETOMI development (Step 2). POMINO-TROPOMI data were resampled to 0.05°×0.05° through level-2 products. Other data were downscaled to the same horizontal resolution of 0.05°×0.05° by bilinear interpolation. POMINO-TROPOMI was the target variable (green shade).

Data type	Variable	Abbreviation	Unit	Period
POMINO-TROPOMI	NO_2 TVCDs	tpomino	molec. cm^{-2}	July 2018-Dec. 2020 for training XGBoost model; 2010, 2013-2016, and 2018-2020 for predicting RETOMI2 based on trained XGBoost model
REOMI	Reconstructed NO_2 TVCDs	reomi	molec. cm^{-2}	
Meteorology	2m temperature	t2m	K	
	Boundary layer height	blh	m	
	100-meter eastward wind	u100	m s^{-1}	
	100-meter northward wind	v100	m s^{-1}	
	10-meter eastward wind	u10	m s^{-1}	
	10-meter northward wind	v10	m s^{-1}	
	Surface pressure	sp	hPa	
	Total column ozone concentration	tco3	du	
	2-meter dew point temperature	d2m	K	
	Total Trop. column water	tcw	g cm^{-2}	
	Total column water vapor	tcwv	g cm^{-2}	
Socio-economic	Gridded population	pop	people/grid	
Land use	Proportion of crop	cropland	%	
	Proportion of impervious surface	impervious surface	%	
	Proportion of water	water	%	
	Proportion of forest	forest	%	
Spatiotemporal information	Longitude	lon	°	
	Latitude	lat	°	
	Day of year	doy	-	
	Day of week	dow	-	

Table S10. Summary of data used for AKs estimation. POMINO-TROPOMI data were resampled to 0.05°×0.05° through level-2 products. Other data were downscaled to the same horizontal resolution of 0.05°×0.05° by bilinear interpolation. POMINO-TROPOMI was the target variable (green shade).

Data type	Variable	Abbreviation	Unit	Period
POMINO-TROPOMI	Daily averaging kernels	tpomino-ak	Unitless	July 2018-Dec. 2020 for training XGBoost model; 2010, 2013-2016, and 2018-2020 for predicting REAK based on trained XGBoost model
POMINO	Daily averaging kernels	pomino-ak	Unitless	
Meteorology	2m temperature	t2m	K	
	Boundary layer height	blh	m	
	100-meter eastward wind	u100	m/s	
	100-meter northward wind	v100	m/s	
	10-meter eastward wind	u10	m/s	
	10-meter northward wind	v10	m/s	
	Surface pressure	sp	hPa	
	Total column ozone concentration	tco3	du	
	2-meter dew point temperature	d2m	K	
	Total Trop. column water	tcw	g/ cm^2	
	Total column water vapor	tcwv	g/ cm^2	
Socio-economic	Gridded population	pop	people/grid	
Land use	Proportion of crop	cropland	%	
	Proportion of impervious surface	impervious	%	
	Proportion of water	water	%	
	Proportion of forest	forest	%	
Spatiotemporal information	Longitude	lon	°	
	Latitude	lat	°	
	Day of year	doy	-	
	Day of week	dow	-	
Satellite variables	Relative azimuth angle	relazm	°	
	Solar zenith angle	sza	°	
	Viewing zenith angle	vza	°	
	Aerosol optical depth	aod	Unitless	
	Single scattering albedo	ssa	Unitless	
	Effective cloud fraction	cldf	Unitless	
	Cloud radiation fraction	wcld	Unitless	

Table S10. (Continued Table)

Data type	Variable	Abbreviation	Unit	Period
Satellite variables	NO_2 Trop. air quality factor	amf	Unitless	July 2018-Dec. 2020 for training XGBoost model; 2010, 2013-2016, and 2018-2020 for predicting REAK based on trained XGBoost model
	NO_2 Trop. air quality factor (clear-sky)	amfclr	Unitless	
	NO_2 Trop. air quality factor (cloudy-sky)	amfcld	Unitless	
	Temperature of each layer	temp	K	
	Tropopause pressure	troppt	hPa	
	Effective cloud pressure	cldp	hPa	
	Air pressure of each layer	pres	hPa	
	Surface pressure	spin	hPa	

Table S11. The variability of *β* with different levels of emission perturbation, relative to the value with a 10% perturbation of NO_X emissions for 2014 NMD.

Perturbation of NO_X emissions	The variation of β relative to a 10% perturbation
20%	4.04%
30%	5.82%
40%	6.96%
50%	8.03%
60%	9.34%